Article

Development of a Laser Triangulation Displacement Probe with Laser Beam Pointing Control

Hongwei Yang *, Wei Tao, Zhengqi Zhang, Siwei Zhao, Xiaoqia Yin and Hui Zhao

Department of Instrument and Engineering, Shanghai Jiao Tong University, Shanghai, 200240, China; yanghongwei@sjtu.edu.cn (Y.Hw.); taowei@sjtu.edu.cn (T.W.); yehaoyun@sjtu.edu.cn (Z.Zq.); zsw-122@163.com (Z.Sw.); xiaoq1216@sjtu.edu.cn (Y.Xq.); huizhao@sjtu.edu.cn (Z.H.)

* Correspondence: yanghongwei@sjtu.edu.cn; Tel.: +86-21-3420-5931

Abstract: Directional dithering of a laser beam potentially limits the detection accuracy of a laser triangulation displacement probe. A theoretical analysis indicates that the measurement accuracy will linearly decrease as the laser dithering angle increases. To suppress laser dithering, a laser triangulation displacement probe with laser beam pointing control, which consists of a collimated red laser, a laser beam pointing control setup, a receiver lens, and a charge-coupled device, is proposed in this paper. The laser beam pointing control setup is inserted into the source laser beam and the measured object and can separate the source laser beam into two symmetrical laser beams. Hence, at the angle at which the source laser beam dithers, the positional averages of the two laser spots are equal and opposite. Moreover, a laser dithering compensation algorithm is used to maintain a stable average of the positions of the two spots on the imaging side. Experimental results indicate that with laser beam pointing control, the standard variance of the fitting error decreases from 0.3531 to 0.0100, the repeatability accuracy can be decreased from ±7 mm to ±5 μm, and the nonlinear error can be reduced from ±6 %FS to ±0.16 %FS.

Keywords: laser triangulation displacement probe; laser beam pointing; prism.

1. Introduction

Laser triangulation displacement probes (LTDPs) have been widely used for industrial detection because of their noncontact and high-precision properties. The principles of an LTDP are illustrated in Figure 1. A collimated laser beam projects a laser dot onto the measured object. Then, the diffused laser light is collected by a receiver lens, and a dot is imaged on a charge-coupled device (CCD). When the object dot moves in a direction perpendicular to the optical axis of the laser, a corresponding displacement will occur for the image dot on the CCD.

As shown in Figure 1, ε is defined as the observed angle between the source laser beam and the optical axis of the receiver lens, and β is defined as the image angle between the CCD and the optical axis. ε and β must satisfy the Scheimpflug condition [1]. s is the distance over which the object moves, and UL is the corresponding image distance. If s is upward along the optical axis, the sign is "+"; otherwise, it is "-." The relationship between s and UL is

$$UL = \frac{sl' \cdot \sin(\beta)}{l \sin(\beta) \mp s \sin(\varepsilon + \beta)}. \quad (1)$$

The measurement accuracy of the LTDP is affected by the speckle, the color of the measured object, the surface texture, the ambient light, the variation in the laser beam intensity, the distortion of the receiver lens, and the dithering of the source laser beam [2–5]. Shen et al. [6] introduced a digital correlation method for suppressing the speckle noise. The results showed that the measurement range reached 1 μm, and the experimental errors were reduced below 2 %. Oh et al. [7] improved the hardware structure by inserting a diffraction grating between the receiver lens and the CCD. The diffraction grating simultaneously generated −1- and 0-order light intensity distributions on the CCD. This method can reduce the measurement time by averaging the results of the two orders. Jung

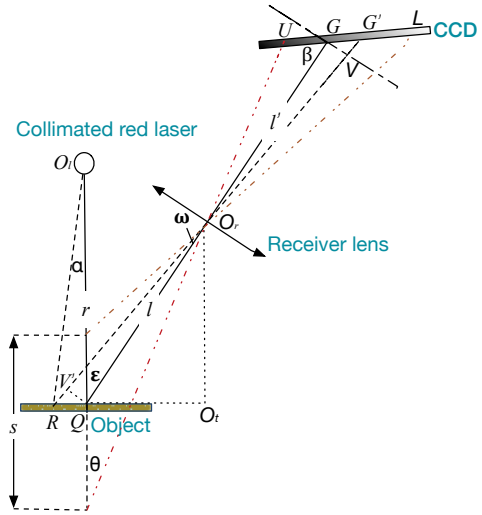

Figure 1. Structure of the optical path when the laser beam is dithered by an angle α.

et al. [8] and Shen et al. [6] interpreted an adaptive control technique to maintain a stable beam intensity. Keyence [9] proposed a real peak detection algorithm that aimed to detect the true peak position value rather than the traditional centroid value to avoid the effect of the oversized diameter. Zbontar et al. [10] introduced a double curve fitting algorithm to compensate the skewed distribution. In addition, they [10] used an ultraviolet (UV) laser to improve the required signal quality. However, the UV laser will induce photochemical effects, which might lead to material degeneration; thus, this method is only used to detect certain materials such as high-end lenses or hot metals.

In this paper, an LTDP that uses a laser beam pointing control setup (LPC) is proposed to decrease the effect of directional dithering of a laser beam. This probe simultaneously generates two symmetrical laser intensity distributions. Since the averages of the two positions on the detected surface are constant, the influence of laser dithering can be avoided. Moreover, the speckle noise related to the measured surface roughness and stray light can be reduced because the two measurement results are averaged.

The remainder of the paper is arranged as follows. We analyze the effect of laser dithering on the measurement accuracy of an LTDP in Section 2. Section 3 describes the LTDP with the LPC and introduces the laser dithering compensation algorithm. Experiments for verifying the performance of the probe are presented in Section 4. Finally, the conclusions are summarized in Section 5.

2. Effect of the Laser Beam Directivity on the Measurement Accuracy

Figure 2(a) and Figure 2(b) show two different occurrences of laser dithering produced by two different collimated lasers manufactured by Xi'an Minghui Optoelectronic Technology Co., Ltd. The experimental results show that the laser dithering angle is usually within $(-1°, 1°)$.

The relationship between the dithering angle and the imaging error is deduced as follows. As shown in Figure 1, a stable pointing laser source emits the light spot Q on an object. The diffused light is collected by a receiver lens, and the light spot G is imaged on the CCD. When the source laser beam is dithered by the angle α, the light spot R is projected onto the object. Then, the diffused light is collected, and the light point $G^{'}$ is imaged on the CCD. The angle between the rays O_lQ and O_lR is defined as α, and the angle between the rays RO_r and QO_r is defined as ω. Moreover, the auxiliary line GV, which is perpendicular to the ray QG, and the auxiliary line $QV^{'}$, which is perpendicular to the ray QG, are added separately.

$\angle V^{'}RQ = 90° - (\omega + \angle QO_rO_t) = 90° - \omega - \varepsilon$; considering $\triangle RV^{'}Q$ in Figure 1, by the law of sines,

Preprints (www.preprints.org) | NOT PEER-REVIEWED | Posted: 30 March 2017 doi:10.20944/preprints201703.0221.v1

Peer-reviewed version available at Sensors 2017, 17, , 1126; doi:10.3390/s17051126

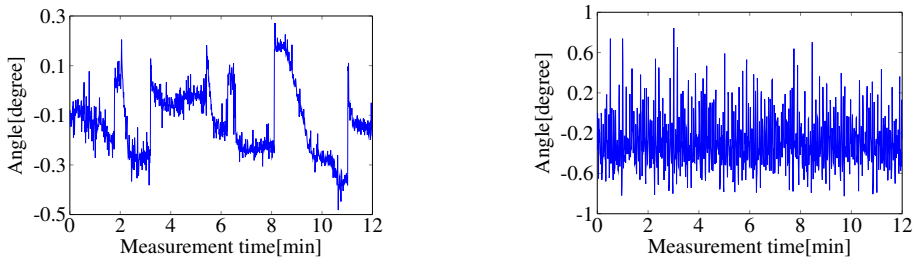

Figure 2. Laser beam pointing images captured by a beam profiler (BP100, Thorlabs., Inc.). (**a**)Green laser. λ=520 nm, and the power is 4.6 mW. (**b**)Red laser. λ =635 nm, and the power is 2.1 mW.

$$\frac{\overline{QR}}{\sin(90^\circ+\omega)} = \frac{\overline{QV'}}{\sin(90^\circ-\omega-\varepsilon)} \Rightarrow \overline{QV'} = \frac{\cos(\omega+\varepsilon)}{\cos\omega}\overline{QR}. \tag{2}$$

Since $\triangle V'QO_r \sim \triangle GVO_r$, $\overline{QV'}$ is expressed as follows:

$$\overline{GV} = \frac{l'}{l}\overline{QV'}, \tag{3}$$

where l is the length of $\overline{QO_r}$, and l' is the length of $\overline{O_rG}$. Using Equation 2,

$$\overline{GV} = \frac{l'}{l}\frac{\cos(\omega+\varepsilon)}{\cos\omega}\overline{QR}. \tag{4}$$

In $\triangle\, O_rO_tR$, $\omega+\varepsilon = \tan^{-1}(RO_t/O_rO_t)$. In $\triangle\, O_lRQ$, $\overline{QR} = r\cdot\tan\alpha$; thus, ω is expressed as follows:

$$\omega = \tan^{-1}\frac{\overline{RO_t}}{\overline{O_rO_t}} - \varepsilon = \tan^{-1}\frac{r\cdot\tan\alpha + l\cdot\sin\varepsilon}{l\cdot\cos\varepsilon} - \varepsilon = Z - \varepsilon, \tag{5}$$

where $Z = \tan^{-1}(r\cdot\tan\alpha + l\cdot\sin\varepsilon)/(l\cdot\cos\varepsilon)$. Combining Equation 4 and Equation 5, $\overline{GV}$ is expressed as follows:

$$\overline{GV} = T\cdot r\cdot\tan\alpha\cdot\frac{\cos Z}{\cos(Z-\varepsilon)}, \tag{6}$$

where $T = l/l'$.

Considering the inclination angle β of the CCD, the relationship between the dithering angle α and the dithering error $\triangle x$ over the distance GG' on the image side can be written as follows:

$$\triangle x = T\cdot r\cdot\tan\alpha\cdot\frac{\cos Z}{\cos(Z-\varepsilon)}\cdot\frac{\cos\omega}{\sin(\beta-Z+\varepsilon)}. \tag{7}$$

The relationship between $\triangle x$ and α is shown in Figure 3 for $l' = 59$ mm, $l = 68.5$ mm, $r = 60$ mm, $\varepsilon = 0.349$, $\beta = 0.5916$, and $\alpha \in (-1^\circ, 1^\circ)$.

Preprints (www.preprints.org) | NOT PEER-REVIEWED | Posted: 30 March 2017 doi:10.20944/preprints201703.0221.v1

Peer-reviewed version available at Sensors 2017, 17, , 1126; doi:10.3390/s17051126

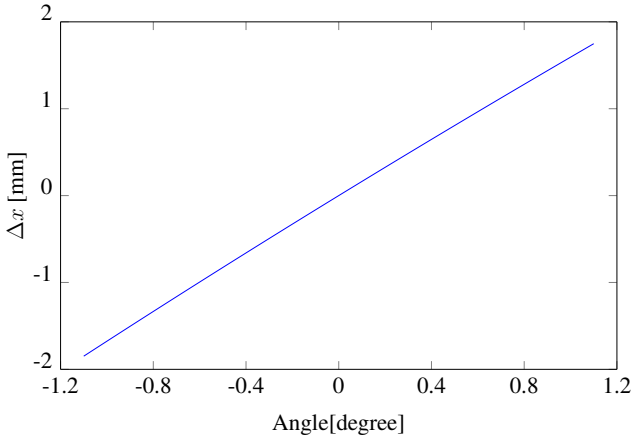

Figure 3. Relationship between $\triangle x$ and the dithering angle α.

As shown in Figure 3, when the source laser beam is dithered by an angle of -1° to 1°, the measurement accuracy will decrease linearly as the dithering angle increases.

3. Measurement Methodology

3.1. Basic Layout

To avoid the effect of laser dithering, several effective methods have been proposed. In general, these methods utilize feedback control achieved by using the error or reference signal [11–15]. However, these methods are inappropriate for an LTDP because the structures mentioned in these studies have a large volume and there is a dependence on the error or reference signal. Therefore, an LTDP based on laser beam pointing control is designed in this study, which consists of a collimated red laser, an LPC, a receiver lens, and a CCD, as shown in Figure 4.

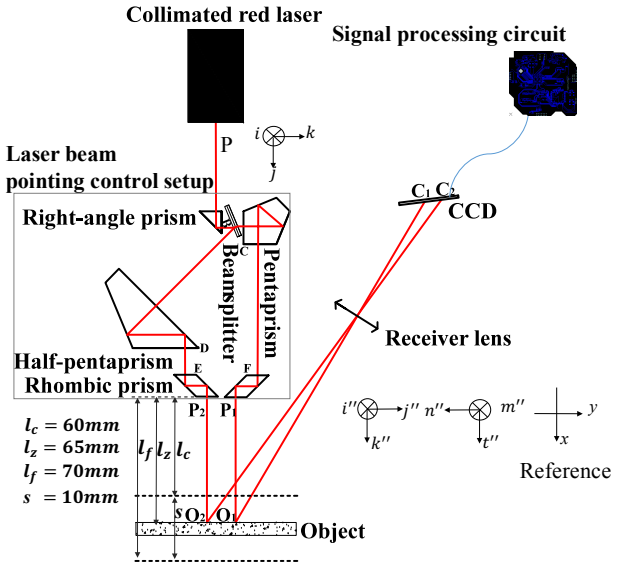

Figure 4. Optical structure of the laser triangulation displacement probe with laser beam pointing control.

The LPC consists of a right-angle prism, a beam splitter, a pentaprism, a half-pentaprism, and two rhombic prisms. The angle between the beam splitter and the optic axis of the collimated red laser is 22.5°. The collimated red laser beam is reflected by the right-angle prism and split into

Peer-reviewed version available at Sensors 2017, 17, , 1126; doi:10.3390/s17051126

two laser beams by the beam splitter. One laser beam is reflected four times by the pentaprism and rhombic prism, and the laser beam P_1 is formed. Another laser beam is reflected four times by the half-pentaprism and another rhombic prism, and the laser beam P_2 is formed. The two rhombic prisms can shorten the distance traveled by the two laser beams, which are located at positions perpendicular to the optical axes of P_1 and P_2.

With respect to the LPC, the closer point, zero point and farther point were set at distances of 60 mm, 65 mm and 70 mm with an error of 0.2 mm.

(i, j, k) is defined as the unit vector of the source laser beam P, and (i'', j'', k'') is the unit vector of P_1. According to the prism turning theorem, the interaction matrix B_1 of P_1 is

$$B_1 = \begin{bmatrix} 1 & 0 & 0 \\ 0 & -1 & 0 \\ 0 & 0 & 1 \end{bmatrix}. \tag{8}$$

Furthermore, (m'', n'', t'') is the unit vector of P_2, and the interaction matrix B_2 of P_2 is

$$B_2 = \begin{bmatrix} 1 & 0 & 0 \\ 0 & 1 & 0 \\ 0 & 0 & 1 \end{bmatrix}. \tag{9}$$

Comparing Equation 8 and Equation 9, the basis vector j'' of B_1 and n'' of B_2 are opposite, which means that the directions of P_1 and P_2 are opposite.

To ensure that the positional variations in O_1 and O_2 are equal, the positional relationship among the right-angle prism, pentaprism, half-pentaprism, and rhombic prisms must satisfy

$$\begin{aligned} &|x_1 + x_3 - x_2 + y_3| = \sqrt{2L^2 + h^2 - 2Lh[\cos(22.5^\circ) - \sin(22.5^\circ)]}, \\ &l_1 = 2l_2, \\ &x_E = x_F, \end{aligned} \tag{10}$$

where $L = [x_1 - y_1 + y_2 - x_2 - \sqrt{2} \cdot (x_1 + y_1)]^{1/2}$, (x_1, y_1) are the coordinates of point B, (x_2, y_2) are the coordinates of point D, (x_3, y_3) are the coordinates of point C, $2h$ is the thickness of the beam splitter, l_1 is the length of the short side at 45° in the half-pentaprism, l_2 is the length of the side at 90° in the pentaprism, x_E is the x coordinate of point E, and x_F is the x coordinate of point F. In summary, if the positional relationship of the prisms satisfy Equation 10, the average value of O_1 and O_2 remains invariant.

3.2. Laser Dithering Compensation Algorithm

As shown in Figure 5, a coordinate system (Oxy) is constructed, where O is the medial point of the receiver lens, and the x axis is coincident with the plane of the receiver lens. The linear function of the CCD is defined as $y = k_1 x + b_1$, where $k_1 = \tan \varphi_1$. Point A is the position at which the pixel value on the CCD is *zero*.

The laser dithering compensation algorithm is described as follows. First, the peak value y_{P_1} and the corresponding pixel value x_{P_1} of the point C_1 as well as the peak value y_{P_2} and the corresponding pixel value x_{P_2} of the point C_2 are found. Then, the centroids C_{d_1} and C_{d_2} of C_1 and C_2, respectively, are calculated using

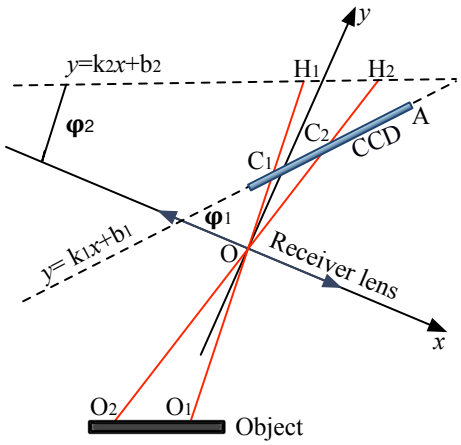

Figure 5. Working principle of the laser dithering compensation algorithm.

$$
\begin{aligned}
C_{d_1} &= \frac{\sum_{i=x_{P_1}-w}^{x_{P_1}-1} x_i \cdot y_i + x_{P_1} \cdot y_{P_1} + \sum_{j=x_{P_1}+1}^{x_{P_1}+w} x_j \cdot y_j}{\sum_{i=x_{P_1}-w}^{x_{P_1}-1} y_i + y_{P_1} + \sum_{j=x_{P_1}+1}^{x_{P_1}+w} y_j}, \\
C_{d_2} &= \frac{\sum_{p=x_{P_2}-w}^{x_{P_2}-1} x_p \cdot y_p + x_{P_2} \cdot y_{P_2} + \sum_{q=x_{P_2}+1}^{x_{P_2}+w} x_q \cdot y_q}{\sum_{i=x_{P_2}-w}^{x_{P_2}-1} y_q + y_{P_2} + \sum_{q=x_{P_2}+1}^{x_{P_2}+w} y_q},
\end{aligned}
\tag{11}
$$

where w is the data width, i is the pixel value before x_{P_1}, j is the pixel value after x_{P_1}, p is the pixel value before x_{P_2}, and q is the pixel value before x_{P_2}.

The x coordinates of C_1 and C_2 in the (Oxy) system are then expressed as follows:

$$
\begin{aligned}
x_{C_1} &= x_A - t \cdot C_{d_1} \cdot \cos\varphi_1, \\
x_{C_2} &= x_A - t \cdot C_{d_2} \cdot \cos\varphi_1,
\end{aligned}
\tag{12}
$$

where x_A is the x coordinate of point A, and t is the resolution of the CCD.

Since the CCD is not parallel to the plane of the object but forms an angle φ_1, the medial position of x_{C_1} and x_{C_2} is not appropriate for calibration. Here, we construct a virtual calibrated line $y = k_2x + b_2$, which is parallel to the plane of the object, as shown in Figure 5, where $k_2 = \tan\varphi_2$.

The x coordinate x_1 of the point H_1 and the x coordinate x_2 of the point H_2 are

$$
\begin{aligned}
x_1 &= \frac{x_{C_1} \cdot b_2}{(k_1 - k_2) \cdot x_{C_1} + b_1}, \\
x_2 &= \frac{x_{C_2} \cdot b_2}{(k_1 - k_2) \cdot x_{C_2} + b_1}.
\end{aligned}
\tag{13}
$$

As a result, the medial position AVG of x_1 and x_2 is

$$
AVG = \frac{x_1 + x_2}{2}. \tag{14}
$$

Since the positional variations in O_1 and O_2 are equal and opposite, the value of AVG remains constant.

4. Experimental Test

4.1. Presetting

An LTDP with an LPC is shown in Figure 6, where the LPC is inserted between the collimated red laser and the detected object. The main devices used in this system are shown in Table 1.

According to the design parameters of the LTDP, the linear function of the CCD is $y = 0.6009x + 46.09$, and the virtual calibrated line is $y = 0.6745x + 46.09$.

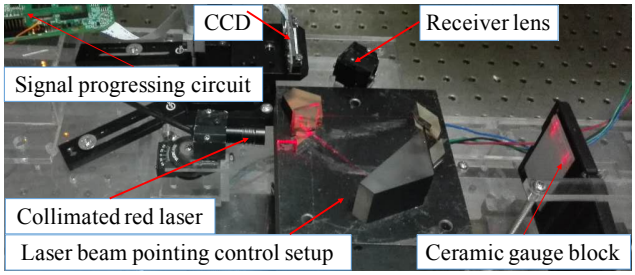

Figure 6. Laser triangulation displacement probe with laser beam pointing control.

Table 1. Devices.

Device	Manufacturer	Type	Major parameters[1]
CCD	Toshiba	TCD2566BFG	Resolution 5.25 µm
Ceramic gauge block	Seeman	WB02	Size 50 × 32 × 4
Red collimated laser	/	KYL635N10-X1240	λ 635 nm
Right-angle prism	Fuyu Optics	/	Size 10 × 10 × 10
Pentaprism	XJT	WJ-151515	Size 15 × 15 × 10
Half-pentaprism	Daheng Optics	/	Size 30 × 30 × 32.6
Rhombic prism	Union Optic	RBP0010	Size 10 × 10 × 14.1
Beam splitter	/	/	Size 10 × 2 × 30
Receiver lens	/	/	Focus 26.054
Rotational devices	Thorlabs	PRM/M	/

[1] All lengths have units of millimeters.

4.2. Verification of the Laser Dithering Compensation Algorithm

Figure 7 shows the values of x_1 and x_2 when the ceramic gauge block is located at one fixed position, and the source laser beam P is rotated within $\pm 1.1°$ with an increment of 0.2°. As shown in Figure 7(a), the variations in x_1 and x_2 are equal and opposite. As shown in Figure 7(b), the extreme error of AVG is within ± 4 µm.

4.3. Calibration

The LTDP with the LPC was calibrated with a RENISHOW XL-80 laser interferometer. The linear resolution of the interferometer is 1 nm. The calibration setup is shown in Figure 8. P_2 is chosen for the comparison of the results. The relative positions of the LTDP with the LPC were calibrated. The criteria ceramic gauge block was moved point-by-point along the optical axis of the source laser beam in an increment of 0.2 mm within 10 mm. At each point, the collimated red laser was rotated with an increment of 0.2° within ±1.1°. Here, AVG is used as the calibration criterion for the LTDP with the LPC, and the pixel value of P_2 is used for the calibration criterion of the LTDP without the LPC. The calibration test results are shown in Figure 9. Figure 9(a) shows the output of the system with the LPC, and Figure 9(b) shows the output without the LPC. Figure 10(a) and Figure 10(b) show the fitting errors for each case.

Preprints (www.preprints.org) | NOT PEER-REVIEWED | Posted: 30 March 2017 doi:10.20944/preprints201703.0221.v1

Peer-reviewed version available at Sensors 2017, 17, , 1126; doi:10.3390/s17051126

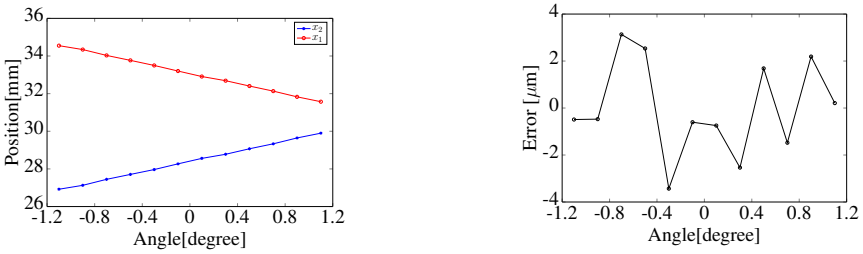

(a) (b)

Figure 7. (**a**) Values of x_1 and x_2. (**b**) Extreme error of AVG.

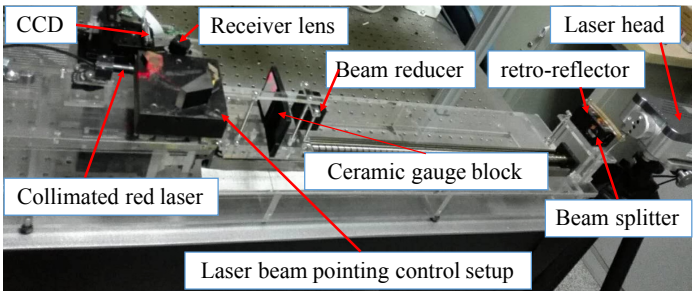

Figure 8. Calibration setup of the laser triangulation displacement probe with laser beam pointing control.

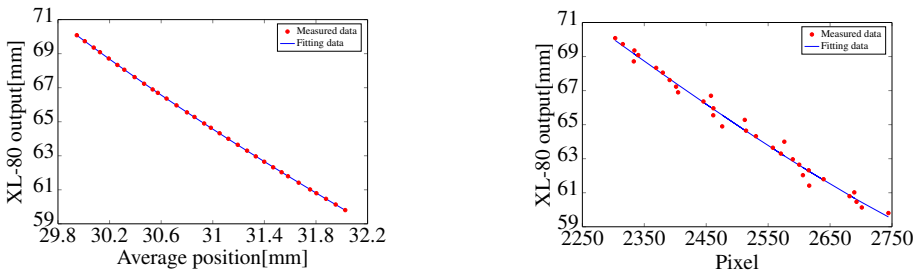

(a) (b)

Figure 9. Calibration results (**a**) with and (**b**) without laser beam pointing control.

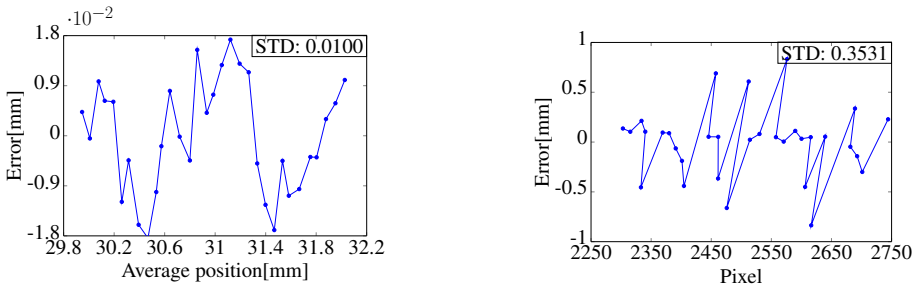

(a) (b)

Figure 10. Fitting errors (**a**) with and (**b**) without laser beam pointing control.

Peer-reviewed version available at Sensors 2017, 17, , 1126; doi:10.3390/s17051126

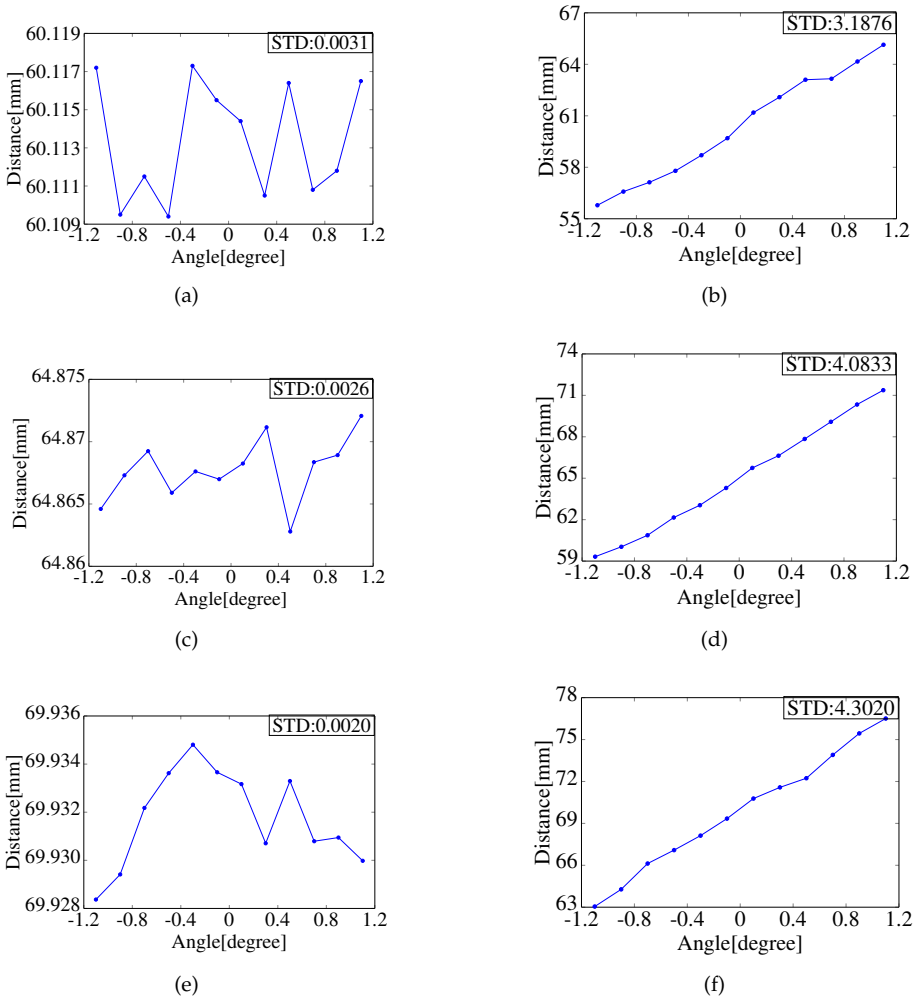

Figure 11. Repeatability (**a**) with and (**b**) without laser beam pointing control when the object is located at a closer point. Repeatability (**c**) with and (**d**) without laser beam pointing control when the object is located at a zero point. Repeatability (**e**) with and (**f**) without laser beam pointing control when the object is located at a farther point.

The results show that the calibration curve of the LTDP with the LPC is coincident with that of the laser interferometer. Moreover, the standard deviation (STD) of the probe is shown in Figure 10. The STD is found to be 0.0100 with the LPC, as shown in Figure 10(a). In comparison, the STD is found to be 0.3531 without the LPC, as shown in Figure 10(b).

4.4. Repeatability Test

As shown in Figure 4, the ceramic gauge block is fixed at a closer point, a zero point, and a farther point. The repeatability of the results with and without the LPC is shown in Figure 11 as the collimated laser is rotated within $\pm 1.1^{\circ}$ with an increment of 0.2°. As shown in Figure 11, the repeatability with the LPC is within $\pm 5\mu m$. In comparison, the repeatability without the LPC is ± 7 mm. Moreover, the STD is decreased by four orders of magnitude with the LPC.

4.5. Nonlinearity Test

The nonlinearity is expressed as $(x_t - x_r)/l_r$, where x_t is the tested value of the LTDP, x_r is the tested value of the XL-80 interferometer, and l_r is the tested range. In this experiment, measurements were performed by moving objects from a closer point to a farther point with an increment of 0.2 mm

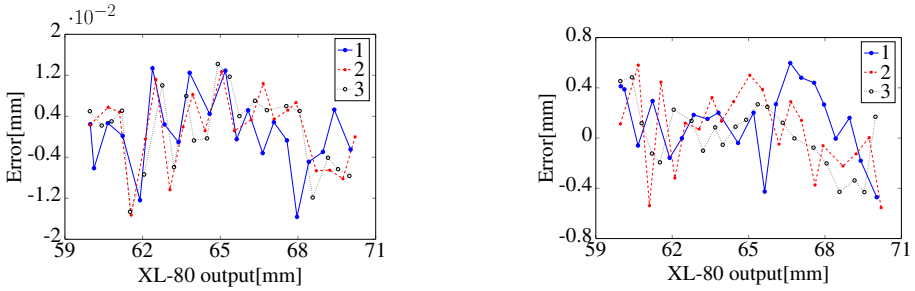

Figure 12. Nonlinearity (**a**) with and (**b**) without laser beam pointing control.

for three runs. The error between the LTDP and the XL-80 interferometer is shown in Figure 12. As the results show, the nonlinearity with the LPC is within ±0.16 %FS. In comparison, the nonlinearity without the LPC is within ±6 %FS.

5. Conclusions

Laser beam dithering is considered one of the major error sources for LTDP measurements. A theoretical analysis shows that the measurement error will increase linearly as the drift angle increases. An LTDP with laser beam pointing control has been developed to decrease the influence of laser beam dithering. This probe consists of a collimated red laser, an LPC, a receiver lens, and a CCD. The collimated red laser beam is split into two symmetrical laser beams by the LPC. Therefore, at the angle at which the laser is dithered, the positional average of two laser spots on the measured object remains constant. The experimental tests were effectively verified with a dual-beam laser interferometer within the measurement range of 10 mm. With laser beam pointing control, the repeatability of the measurement displacement is better than ±5 µm, and the nonlinearity is better than ±0.16 %FS. In comparison, without laser beam pointing control, the repeatability of the measurement displacement is ±7 mm, and the nonlinearity is ±6 %FS.

Acknowledgments: All authors gratefully acknowledge financial support from the Science and Technology Commission of Shanghai Municipality, Shanghai. The project number is 15JC1402500.

Author Contributions: Y.Hw. and T.W. conceived and designed the experiments; Y.H., Z.Zq., and Y.Xq. performed the experiments; Y.Hw. and Z.Z. analyzed the data; T.W. and Z.Sw. contributed materials; and Y.Hw. wrote the paper.

Conflicts of Interest: The authors declare no conflict of interest. The founding sponsors had no role in the design of the study; in the collection, analyses, or interpretation of data; in the writing of the manuscript; and in the decision to publish the results.

References

1. Scheimpflug, T. -scheimpflug, 1904. US Patent 751,347.
2. Dorsch, R.G.; Häusler, G.; Herrmann, J.M. Laser triangulation: fundamental uncertainty in distance measurement. *Applied Optics* **1994**, *33*, 1306–1314.
3. Liu, C.H.; Jywe, W.Y.; Chen, C.K. Development of a diffraction-type optical triangulation sensor. *Applied optics* **2004**, *43*, 5607–5613.
4. Daneshpanah, M.; Harding, K. Surface sensitivity reduction in laser triangulation sensors. SPIE Optical Engineering+ Applications. International Society for Optics and Photonics, 2011, pp. 81330O–81330O.
5. Miks, A.; Novak, J.; Novak, P. Analysis of imaging for laser triangulation sensors under Scheimpflug rule. *Optics express* **2013**, *21*, 18225–18235.
6. Shen, L.; Li, D.; Luo, F. A study on laser speckle correlation method applied in triangulation displacement measurement. *Optik - International Journal for Light and Electron Optics* **2013**, *124*, 4544–4548.
7. Oh, S.; Kim, K.C.; Kim, S.H.; Kwak, Y.K. Resolution enhancement using a diffraction grating for optical triangulation displacement sensors. Symposium on Integrated Optics. International Society for Optics and Photonics, 2001, pp. 102–108.
8. Jung, J.K.; Kang, S.G.; Nam, J.S.; Park, K.H. Intensity Control of Triangulation Based PSD Sensor Independent of Object Color Variation. *Sensors Journal, IEEE* **2011**, *11*, 3311–3315.
9. Inc., K. *LASER DISPLACEMENT SENSOR TECHNOLOGY BOOK*. http://www1.keyence.com/topics/vision/lkg/book.php.
10. Žbontar, K.; Podobnik, B.; Povše, F.; Mihelj, M. On-machine laser triangulation sensor for precise surface displacement measurement of various material types. SPIE Optical Engineering+ Applications. International Society for Optics and Photonics, 2013, pp. 88390M–88390M.
11. Stalmashonak, A.; Zhavoronkov, N.; Hertel, I.V.; Vetrov, S.; Schmid, K. Spatial control of femtosecond laser system output with submicroradian accuracy. *Applied optics* **2006**, *45*, 1271–1274.
12. Singh, R.; Patel, K.; Govindarajan, J.; Kumar, A. Fuzzy logic based feedback control system for laser beam pointing stabilization. *Applied optics* **2010**, *49*, 5143–5147.
13. Jie'an, L.; Xuemei, D.; Jiwen, C.; Jiubin, T. Compensation of laser beam directional stability offset error by using translational spectroscope. Proc. of SPIE Vol, 2011, Vol. 7544, pp. 75441B–1.
14. V.Mitchell, P. Fast Steering Mirror Technology: Active Beam Stabilization. *Newport Corporation* **01-01**, pp. DS–01012.
15. Ding, L.; Li, S.; Lu, Z.; Wang, Y.; Zhu, C.; Chen, Y.; Du, P.; Cui, C.; Zhou, L.; Yuan, H.; others. Analysis of the beam-pointing stability in the high power laser system. *Optik-International Journal for Light and Electron Optics* **2016**, *127*, 6056–6061.